TOPOGRAPHIC CONTROL OF OCEANIC FLOWS IN DEEP PASSAGES AND STRAITS

J. A. Whitehead
Department of Physical Oceanography
Woods Hole Oceanographic Institution
Woods Hole, Massachusetts

Abstract. Saddle points between neighboring deep ocean basins are the sites of unidirectional flow from one basin to the next, depending on the source of bottom water. Flow in these sites appears to be topographically controlled so the interface between the bottom water and the water above adjusts itself to permit bottom water flow from the basin that contains a source of bottom water into the next. Examples in the Atlantic include flow in the Romanche Fracture Zone, the Vema Channel, the Ceara Abyssal Plain, the Anegada-Jungfern passage, and the Discovery Gap, but there are many more. Theoretical predictions of volume flux using a method that requires only conductivity-temperature-depth data archives and detailed knowledge of bathymetry near the saddle point are compared with volume flux estimates using current meters and/or geostrophic estimates for seven cases. The ratio of prediction to volume flux estimate ranges from 1.0 to 2.7. Some ocean straits that separate adjacent seas are also found to critically control bidirectional flows between basins. Theory of the influence of rotation on such critical flows is reviewed. Predictions of volume flux in eight cases are compared with ocean estimates of volume flux from traditional methods.

1. INTRODUCTION

For over 100 years, topographic control of fluid flowing through constrictions has been studied in a number of situations involving compressible, free surface, stratified or rotating fluid. One relatively recently developed class of these problems combines stratified and rotating constraints on the fluid as it passes over bottom and sidewall constrictions. This class has come to be loosely termed "rotating hydraulics." Problems are typically solved with ocean or atmospheric examples in mind.

This paper reviews a number of ocean-related aspects of this problem. It does not exhaustively cover all the theoretical studies to date. Rather, the emphasis is on intercomparison of theoretical predictions of volume flux with oceanographic estimates based on direct measurements. The intent is to assess the practical usefulness of the theory presented here to knowledge of the ocean through quantitative comparison between data and calculations.

We first describe the simplest concept of critical control of a nonrotating fluid. Consider a simple frictionless fluid flow problem as sketched in Figure 1, where water with a surface that is free to deform in a field of gravity of depth H and velocity V is flowing along a channel (just like water flowing in a river). We take this to be a specified upstream state. Now let us find its response as it encounters a bump of size b. The fluid must conserve mass as it flows over the bump. Since we approximate water as incompressible for such applications in the ocean, the mass flux conservation is equivalent to constancy of volume flux along the channel in steady state. If the surface of the fluid were to remain flat over the bump, the fluid would have to speed up to maintain the same volume flux. In addition, an inviscid fluid speeding up has lower pressure (often called the "Venturi effect"). Thus one might expect a free surface to be lower over the bump, as is sketched at the top of Figure 1. It is well known that this happens as long as the upstream flow is below a certain speed. As the bump becomes bigger, progressively lower surface height is expected.

Naturally, bump height cannot be increased indefinitely. It certainly cannot be great enough to meet the lowered surface, since in that case no volume flux could pass over the bump. In fact, the bump reaches a certain height (called "critical height") which causes a dilemma. For bump heights above this value the volume flux, which is a product of (finite) velocity and water depth (from lowered surface to the top of the bump) cannot exist at the upstream value.

The only resolution is for some upstream condition to be changed. Velocity V could be changed, keeping H constant, or H could be changed, keeping V constant. In either case the product VH is changed. Usually, in a physical problem the upstream state will change to the value that produces a critical height at the bump. In that case the upstream conditions are said to be "critically

Reviews of Geophysics, 36, 3 / *August 1998*
pages 423–440
8755-1209/98/98RG-01014*$15.00*
Paper number 98RG01014

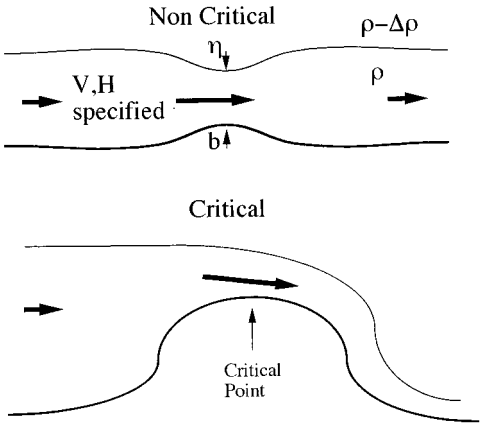

Figure 1. Sketch of an idealized flow of fluid along a channel with upstream velocity V and depth H, and the adjustment to a slowly increasing bottom b. The deflection downward of the interface is h.

controlled" by the bump. If the bump were to become even slightly shallower, the upstream state would have to change yet again. When flow is critically controlled, it possesses different interface profiles upstream and downstream of the bump as shown at the bottom of Figure 1.

The state shown at the bottom of Figure 1 can occasionally be found in physical oceanography. Dense water accumulates in a basin from either surface cooling (in polar latitudes), inflow from an adjacent basin, or surface evaporation. The water above sill depth then flows out through the passage. We infer that as the dense water accumulates, the interface of the dense water rises until it is above sill depth of the deepest passage that drains the dense water to another basin. When the outflow rate equals the accumulation rate of dense water, the interface ceases to rise and steady state is achieved. Volume flux of such outflows are useful measurements of interbasin water exchange. Hence they are of fundamental interest in physical oceanography and ocean climate considerations.

We review here some theoretical studies of the critical control problem for rotating fluids with possible ocean applications. All have been conducted over the past 25 years. Geometries include not only deep passages, which we will call "sills" where one water mass flows between basins, but also surface passageways (straits) where flows in both directions interchange water masses. A particular case in which there are boundaries with many gaps, so that one strait might support flow in one direction, but return flow is elsewhere (as elucidated by *Nof and Olson* [1983] and *Nof* [1995a, b]), will not be reviewed here. Sections 2 and 4 summarize theoretical aspects of sill flows and long strait flows, respectively. Sections 3 and 5 discuss ocean observations of such flows and some comparison with theory.

2. SILL FLOW CALCULATIONS

As in our introduction, we take as our starting point inviscid equations of steady fluid motion including frame rotation. The rotation vector is aligned with gravity for simplicity. The equations of momentum are

$$\mathbf{u}' \cdot \nabla \mathbf{u}' + f\hat{k} \times \mathbf{u}' = -\frac{1}{\rho} \nabla p - g\hat{k} \tag{1}$$

and conservation of incompressible volume flux is

$$\nabla \cdot \mathbf{u}' = 0 \tag{2}$$

where $\mathbf{u}'$ is fully three dimensional. The primary justification of using four terms in (1) is simplicity (Occam's razor). Put another way, everything is included that is needed to discuss the issue, but nothing is added to distract us from the issue.

Restricting flow to two layers separated by an interface at $z = h(x, y)$, with density of the motionless top fluid being ρ and the bottom fluid being $\rho + \Delta\rho$, and assuming slow variation of flow in the lateral directions, (1) and (2) reduce to a "reduced gravity" expression for flow in the bottom layer

$$\mathbf{u} \cdot \nabla \mathbf{u} + f\hat{k} \times \mathbf{u} = -\frac{g\Delta\rho}{\rho} \nabla h \tag{3}$$

where $\mathbf{u}$ is two-dimensional in the horizontal plane.

The first term in (3) represents the transport of momentum by the fluid. It corresponds to the force due to inertia of the fluid as it is moved from place to place. The second term corresponds to the alteration of momentum as fluid flows in a rotating system. It is called the "Coriolis force" and acts at right angles to a fluid element that moves in a rotating frame. The third term is simple pressure whose gradient produces a force on an element of fluid. Other forces that could be included in more complicated models (and that require additional terms in (3)) are acceleration, friction, effects of large vertical motion, and eddy Reynolds stress. These are all left out of this simplest case. It is easily shown that the terms in (3) are the leading terms when changes are sufficiently slow (time $\gg L/V$, where L is a lateral length scale; where the vertical length scale is sufficiently small ($H \ll L$); and where viscosity ν is sufficiently weak ($VL/\nu \gg 1$)).

Figure 2 shows the balance of these three forces (Coriolis, inertia, and pressure) that are included in the simplest problems of rotating hydraulic control. These three forces are easily transformed into three well-known relations: The first is the Coriolis force balance with a pressure gradient force. This is frequently called a geostrophic relation. This balance must be satisfied at right angles to the flow direction since Coriolis force acts at right angles to velocity. The second relation is conservation of potential vorticity. This is found by taking the curl of equation (3) and using continuity. Vorticity ζ is the curl of the velocity vector. Potential vorticity for this simple approximation is given in Figure 2, where F

is constant. It represents the total vorticity of a fluid column $\zeta + f$ divided by its depth h. Note that the vorticity of a fluid at rest in a rotating frame is f. Potential vorticity is frequently conserved by flows and is often an extremely useful constraint in geophysical fluid dynamics [*Pedlosky*, 1979]. The third relation is Bernoulli's law, which denotes a balance between the change of momentum ($\rho\mathbf{u}$) and pressure. Although momentum is constant at each spot when the flow is steady, the value of momentum of a fluid parcel can change as it moves from place to place, as is expressed by the first term in equation (3). Bernoulli's law is found by looking at the balance in the direction of flow. The Coriolis force is zero in this direction, since it acts at right angles to velocity. These three relations are redundant, and the cross–stream function derivative of the upstream Bernoulli's function must be equal to the upstream potential vorticity. In the first pioneering attempt to calculate critical flow along a channel [*Stern*, 1972] the basic flow obeyed this constraint, but alterations caused by bottom changes did not.

In the absence of rotation, simple manipulation leads to some insight into topographic control. The equations reduce to Bernoulli's equation and conservation of mass,

$$\tfrac{1}{2}v^2 - g\eta = \tfrac{1}{2}V^2 \tag{4}$$

$$v(H - b - \eta) = VH \tag{5}$$

where v is velocity of fluid over the bump and η is downward deflection of the free surface over the bump. These two equations can be combined by eliminating v to produce the following cubic relation between scaled surface deflection $\eta' = \eta/H$, bottom bump $b' = b/H$, and upstream Froude number $F = V/\sqrt{2gH}$.

$$(1 - \eta' - b')^2 = \frac{1}{1 + (\eta'/F^2)} \tag{6}$$

F is obviously a measure of the ratio of inertia to pressure. However, it is also a measure of velocity magnitude to wave speed (since waves also balance inertia and pressure, but in time-dependent problems).

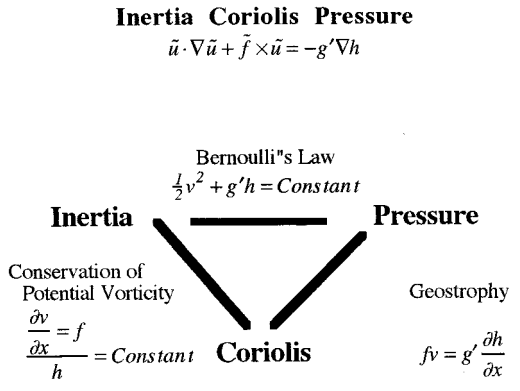

Figure 2. Diagram showing the three forces exerted on a fluid element and how dynamic relations are derived from these three forces.

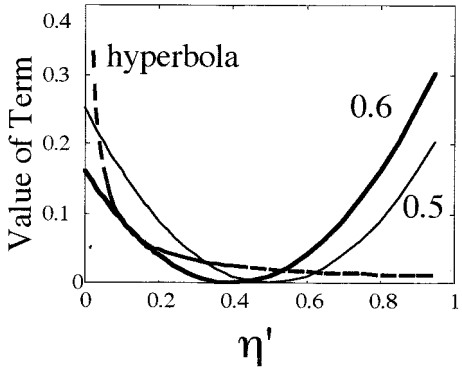

Figure 3. Values of the right and left hand side (a hyperbola and parabola, respectively) of equation (6). The hyperbola (dashed line) is drawn for $F = 0.1$. The rightmost parabola (solid curve) corresponds to $b' = 0.5$. The leftmost parabola (solid heavy curve) corresponds to $b' = 0.6$.

An easy way to picture these solutions is to investigate the intersection of the left-hand parabola of equation (6) with the right-hand hyperbola, keeping η' a freely varying parameter with fixed values of b' and F. Two such examples are shown in Figure 3, both using a hyperbola with $F = 0.1$. The first, represented by the right parabola, has $b' = 0.5$. There are three points of intersection. The leftmost point is the physically realized solution. It corresponds to the small deviation of η as drawn in Figure 1. This is the physically expected solution, since η' continuously maps to zero as b' approaches zero. The middle point is a very much larger value η'. In such a case it can be shown that the velocity divided by wave speed based on local fluid depth (a "local" Froude number F_l) is greater than 1. Surface gravity waves would only radiate in the direction of flow. This state is known as a conjugate state. However, it is unstable [*Pratt*, 1984a] when such a flow lies at the top of a bump. The right intersection point is not physical, since $b' + \eta' > 1$, so the free surface would be below the bottom of the bump.

The left parabola in Figure 3 is shown for $b' = 0.6$; the parabola has simply moved to the left by 0.1 unit of η'. At this value of F, the parabola intersects the hyperbola at only two points. The left point is the critical point and is located where the hyperbola and parabola are tangent. Both left and middle points for $b' = 0.5$ have moved toward each other and merged at this point. In addition, the local Froude number $F_l = 1$ at this point. The right point is still impossible.

For larger values of b' at the same value of F there is no intersection except for the right-hand (impossible) one. Thus if b' is greater than a given value (depending on F), the fluid cannot get over the bump. The physical resolution to this dynamic dilemma is that one of the upstream conditions must be changed. For example, if volume flux is specified, H would need to be bigger.

TABLE 1. List of Theories

Study	*Theory*
Stern [1972]	flow in a channel
Whitehead et al. [1974]	zero potential vorticity, zero current upstream, laboratory confirmation
Sambuco and Whitehead [1976]	very wide channel
Whitehead and Porter [1977]	axisymmetric withdrawal
Gill [1977]	constant potential vorticity, upstream currents found to be necessary
Rydberg [1980]	local F should equal 1, asserted
Shen [1981]	zero potential vorticity, more tests, laboratory confirmation
Pratt [1983]	adjustment to obstacle, properties of waves
Pratt [1984b]	flow near critical speed, waves during adjustment
Borenäs and Lundberg [1986]	parabolic channel
Pratt and Armi [1987]	nonuniform potential vorticity, complicated upstream states
Whitehead [1989]	comparison of zero and const. potential vorticity, application
Dalziel [1988, 1990]	zero potential vorticity exchange and control, two directions
Pratt and Lundberg [1991]	review of theories
Hunkins and Whitehead [1992]	constant potential vorticity exchange, two directions
Killworth [1992]	zero potential vorticity and shapes, application
Killworth and McDonald [1993]	zero potential vorticity and maximum flux
Killworth [1994]	zero potential vorticity is maximum
Johnson and Ohlsen [1994]	frictionally modified exchange
Whitehead and Kimura [1994]	wide exchange flow
Borenäs and Pratt [1994]	comparisons of zero and constant potential vorticity

Alternatively, if H is fixed (for instance by a large upstream lake), V may have to change to allow a flow. Often, the fluid over the bump adjusts to the critical state. In such cases the topography determines what is happening upstream.

This is why such problems are of interest in physical oceanography: a small topographic region may determine conditions (such as the depth for a particular range of water temperature and salinities) for an entire upstream ocean. For such problems involving a rotating fluid, flow in the sill region is usually calculated by using any two of the three equations shown in Figure 2. If the geostrophic and potential vorticity equation are used, for example, two constants of integration are introduced. However, the use of the third (Bernoulli's) equation eliminates one of them, and the last constant is determined using a critical condition. This yields a prediction for flow at the controlling point. Flows elsewhere could then be found using the general equations for Figure 2, and of course, upstream conditions such as H can be found. We show for illustration here the simple theory of zero potential vorticity. Fluid of density $\rho + \Delta\rho$ lies in an infinitely deep upstream basin with surface h_u above the lip of a rectangular exit channel. Above it is motionless fluid of density ρ. The upper fluid has negligible dynamics except that it reduces the restoring force between layers. It is frequently called a $1\frac{1}{2}$ layer problem. This problem has very simple algebraic solutions that illustrate the flows in the channel [*Whitehead et al*., 1974].

The geostrophic equation and zero potential vorticity equation are

$$g' \frac{\partial h}{\partial x} = fv \tag{7}$$

$$\frac{\partial v}{\partial x} = -f \tag{8}$$

which integrate to

$$h = -\frac{f^2x^2}{2g'} + \frac{fv_0x}{g'} + h_0 \tag{9}$$

$$v = -fx + v_0 \tag{10}$$

where $g' = g\Delta\rho/\rho$, f is the Coriolis parameter, and h_0 and v_0 are two constants of integration. They represent water depth and velocity at $x = 0$. In this example, Bernoulli's law exists along each streamline

$$v = \sqrt{2g'(h_u - h)} \tag{11}$$

which can eliminate one constant of integration by making it a function of the other. Note that Bernoulli potential is $g'h_u$, since fluid is stagnant in the upstream basin. In problems with finite values of upstream depth, (i.e., constant upstream potential vorticity [*Gill*, 1977; *Pratt and Armi*, 1987; *Whitehead*, 1989]), Bernoulli's law still holds along all streamlines, but the Bernoulli potential varies from one streamline to another (i.e., is not uniform and is not easy to determine). Fortunately, there are some cases where it can be determined for one or two streamlines [*Gill*, 1977], and this leads to some solutions.

In both the example we show here and the uniform potential vorticity case the problem is reduced to determining the remaining constant of integration by imposing a critical condition. The simplest such condition is that volume flux is maximized through the sill, but there are many others. *Gill* [1977] shows why maximum flux

leads to a suitably defined Froude number equal to one, for instance. Maximizing volume flux results in the following predictions for volume flux for a rectangular opening:

$$Q = \frac{g' h_u^2}{2f} \qquad L > \left(\frac{2g' h_u}{f^2}\right)^{1/2} \tag{12}$$

$$Q = (\tfrac{2}{3})^{3/2} L \sqrt{g'}\left[h_u - \frac{f^2 L^2}{8g'}\right]^{3/2} \quad \text{otherwise} \tag{13}$$

where L is width of the channel.

The first formula (12) is familiar to many oceanographers. It could be obtained from a simple geostrophic calculation if one assumes first that the fluid height on the right-hand side of the sill (looking downstream in the northern hemisphere) equals the upstream fluid surface height above sill depth h_u, and second that the interface intersects the bottom on the left-hand side. The critical control calculation shows merely that h_u produces maximum flux, but it also allows every element of fluid to use the available upstream potential energy through Bernoulli's equation. The second formula (13) is familiar to hydraulic engineers in the limit of $f = 0$, which was first determined in the last century. It can be found from (6) for small Froude number. As f is increased from 0, it smoothly connects the nonrotating result to equation (12).

Numerous studies, listed in Table 1, go beyond this simple zero potential vorticity theory. If potential vorticity is not zero, the functions expressing velocity, height, and volume flux are more complicated but are still readily found by straightforward calculations. Nevertheless, the connection of Bernoulli potential between upstream and the sill is more challenging. In some cases only one streamline has an easily determined Bernoulli potential from a point upstream to a point on the sill. Nevertheless, the maximum flux can be calculated in many cases. *Gill* [1977] simply specified the existence of appropriate currents in the upstream basin for constant upstream vorticity and graphically determined the volume flux as a function of dimensionless parameters. No analytic solutions were attained. *Whitehead* [1989] was able to find analytic solutions to volume flux for a specific upstream geometry where the upstream current is located next to the left-hand wall (looking downstream) and the right-hand wall is infinitely far from the left-hand wall. Unfortunately, there were no analytic solutions for the maximum value. Contours of nine values of volume flux from the analytic solution are shown in Figure 4. This figure differs from a comparable figure of *Whitehead* [1989, Figure 6], in which negative values of fluid depth were allowed in the computation, so the curves in a region below the volume flux maximum are physically unrealizable. This error does not effect the computation of critical flow, however. The central finding of *Whitehead* [1989] was that volume flux for constant potential vorticity lies within 22% of the flux for the zero potential vorticity solution. This means that the

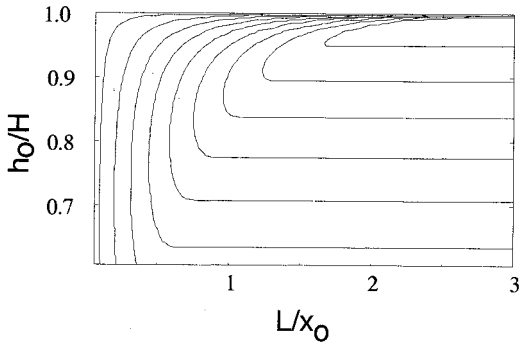

Figure 4. Contours of normalized volume flux $2Qf/g'h_u^2$ as a function of normalized right-hand wall depth and normalized channel width. Contour interval is 0.1. In the region with horizontal contours, the flow does not wet the left-hand wall.

apprehension expressed by *Borenäs and Lundberg* [1988], that the zero potential vorticity assumption was essentially incorrect, is apparently not borne out for issues of volume flux.

Pratt and Armi [1987] investigated the flow patterns in the sill region for more general potential vorticity distributions and found that gyres and countercurrents are possible. Since such cases are characterized by upstream currents, Bernoulli potential varies in the upstream basin, so that comparison of volume fluxes with the simple estimates above is not straightforward. Given these complications, volume fluxes were not determined in these cases, but a variety of issues, such as that the control point is at the crest of the sill for a certain class of sill geometries, were clarified for more general flows.

Rydberg [1980] rejected the maximum volume flux argument (which is equivalent to the Froude number of the longest, fastest wave equal to 1), in favor of having the local Froude number be 1 (i.e., $v/\sqrt{2g'h} = 1$ at every point across the flow). This makes sense because Froude numbers greater than an order 1 constant would produce Kelvin-Helmholtz instability in the $1\frac{1}{2}$ layer problems, which would lead in turn to mixing (Kelvin-Helmholtz instability is the shear instability that grows when Richardson number $g'h/u^2 < \frac{1}{4}$). Unfortunately, there is not yet confirmation of this idea from physical observations. The resolution of this interesting conflict between local and long-wavelength control remains unresolved by either additional theoretical work or direct observation in the laboratory or the ocean.

A simple problem can be solved which uses some information about downstream fluid depth h_d plus channel width w [*Whitehead*, 1986]. Take equations (9) and (10) without reduced gravity (set $g' = g$), so we consider a homogenous fluid flowing in a channel. Next set $h = h_0$ at $x = 0$ to find v_0 on the right-hand wall using equation (11). Finally, set $h = h_d$ at $x = -w$. This assumes that the fastest current is set by the downstream depth. This results in average velocity across the channel being

$$\bar{v} = (2g\Delta h)^{1/2} - \tfrac{1}{2} fw \qquad \text{for} \quad (2g\Delta h)^{1/2}/fw > 1 \tag{14}$$

TABLE 2. Flux Estimates Through Deep Ocean Sills

Sill	*Flux, Sv*	*References*
Denmark Strait	2.9	*Dickson et al*. [1990]; *Dickson and Brown* [1994]
Charlie-Gibbs Fracture Zone	2.4	*Saunders* [1994]
Discovery Gap	0.21	*Saunders* [1987]
Bornholm Strait	0.02	*Petren and Walin* [1976]
Iceland-Faeroe Passage	1.0*	*Dickson et al.* [1990]
Faeroe Bank Channel	1.5–1.9	*Borenäs and Lundberg* [1988]; *Saunders* [1990]
Anegada-Jungfern Passage	0.056	*Stalcup et al*. [1975]
Strait of Sicily†	0.6–0.8	*Morel* [1971]
	0.65	*Molcard* [1972]
	1.23	*Garzoli and Maillard* [1976]
	1.21	*Bethoux* [1979] (using *Whitehead et al*. [1974])
Vema Gap	2.1–2.3	*McCartney et al*. [1991] (using geostrophy)
Ceara Abyssal Plain	0.8–2	*Whitehead and Worthington* [1982]
	>4	*McCartney and Curry* [1993], *Luyten et al*. [1993] (from geostrophy)
	2.0	*Hall et al*. [1997]
Romanche Fracture Zone	1.3	*Polzin et al*. [1996]
Chain Fracture Zone	0.1	*Polzin et al*. [1996]
Vema Channel	4	*Hogg et al*. [1982]
	6	*Speer and Zenk* [1993]
Samoan Passage	1.0, 5.6, 4.8	*Johnson et al*. [1994] (geostrophic estimates)
	6	*Rudnick* [1997]

Other sills include the following: Windward Passage, Amirante Passage, Filchner Depression, southern Weddell Sea, Indonesian-Philippine Basin, Shag Rocks Passage, South Sandwich Island Arc Gap, Ecuador Trench, Panama Basin, and Ninetyeast Ridge.

*Assigned from indirect considerations; no direct measurements are available.

†Values and references are from *Grancini and Michelato* [1987], who did not estimate eastward flow directly but say the current meter data support these hydrographic results.

if v_0 is positive where $\Delta h = h_u - h_d$. If v_0 is negative, there could be a reverse flow in the channel, which would be inconsistent with an upstream source, so we set velocity equal to zero everywhere to the right of the point where $v = 0$. This point is found by setting (10) equal to zero. In that case,

$$\bar{v} = (g\Delta h)/fw \qquad \text{for} \quad (2g\Delta h)^{1/2}/fw < 1 \qquad (15)$$

This was first found by *Garrett and Toulany* [1982], who coined the name "geostrophic control." However, the word "control" is used in a different sense than our usage (see Figure 1) since information about both the geometry of the passage and the downstream height above sill depth h_d is required to solve their problem rather than just geometric information alone. The term "geostrophically determined" seems more accurate to describe equation (15) and "inertially determined" to describe (14). Their concept was extended in various studies [*Garrett*, 1983; *Garrett and Majaess*, 1984; *Toulany and Garrett*, 1984]. In contrast, the first term on the right-hand side of (14) is the classical hydraulic relation for the velocity of flow through a channel. The second, negative term arises from lateral shear due to frame rotation. The important point is that the magnitude of the current as a function of the sea level difference is given by (14), which looks like a modified Bernoulli's law, for $(2g\Delta h)^{1/2} > fw$ and by (15), which looks like a geostrophic balance and the Garrett and Toulany formula in the converse limit. Note that the former limit is valid for large Δh rather than small Δh. If f is fixed in a "run" down problem, the "geostrophic control" comes in more strongly with time. This was also observed experimentally by *Whitehead et al*. [1974]. Note also that when $(2g\Delta h)^{1/2} = fw$, the two results are the same.

The studies by both *Pratt and Armi* [1987] and by *Rydberg* [1980], as well as additional studies by *Borenäs and Lundberg* [1986] and *Gill* [1977], focused strongly upon the implications of the definition of control by the geometry of the outlet passage. This is a rich area of study, since the nature of control from upstream basins with more general vorticity conditions through openings of more general shape is quite complicated. It is easy to visualize, for example, that fluid along a streamline might not possess enough energy to get through an opening while fluid in a streamline nearby could. In that case, upstream blocking might occur that would be connected not with critical control of the entire current, but with current separation. Such a process has the same branch structure used in the aforementioned studies but is distinct from control of the entire current. Another set of physical questions concern the various definitions of critical control. Indeed, Borenäs and Lundberg conclude that there is a range of parameters such that parabolic passageways cannot exert control (in the sense they use the term). Yet it is difficult to imagine that the sketch in Figure 1 breaks down because the channel happens to have a parabolic bottom. Other studies (Table 1) have dealt with a variety of other issues. This review will concentrate on volume flux issues; some of the other

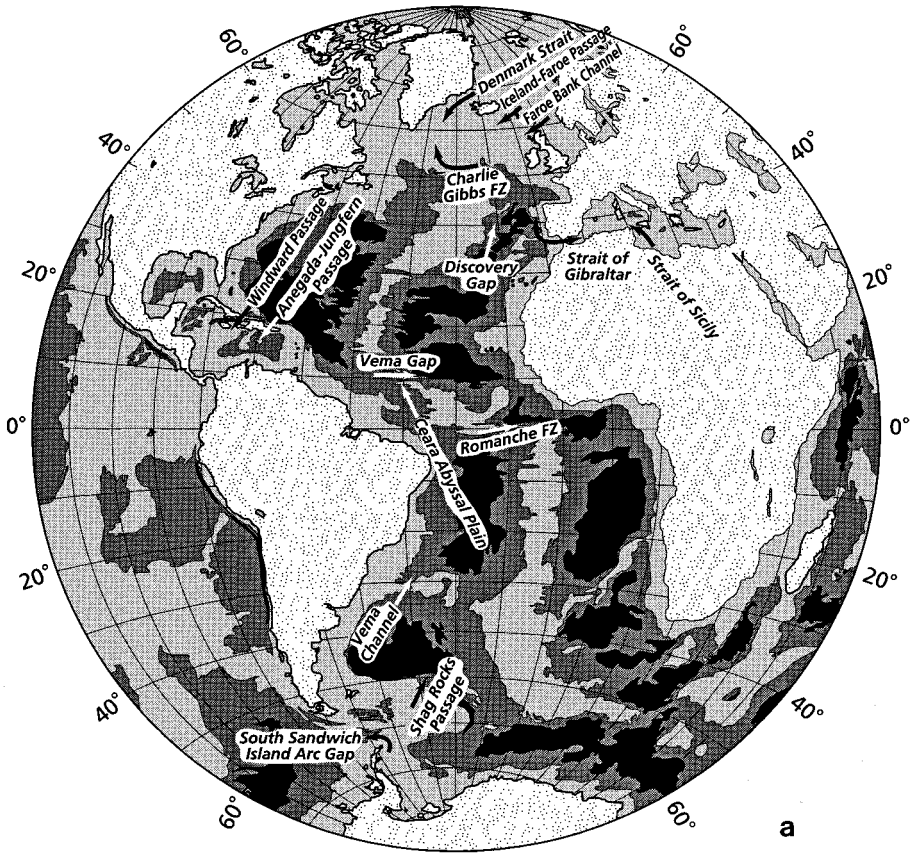

Figure 5. Locations of a number of sills (unidirectional arrows) and straits (bidirectional arrows). (a) Atlantic Ocean with peripheral seas. (b) Pacific Ocean. (c) Indian Ocean. Light grey shading indicates depths of <4000 m; black indicates depths of >5000 m.

issues are covered by *Pratt and Lundberg* [1991] and *Borenäs and Pratt* [1994].

Most quantitative comparisons indicate that neither the potential vorticity distribution nor the shape of the sill produces very large changes (greater than tens of percent) in the volume flux, but they unquestionably produce changes of a fraction of order 1. Recently, *Killworth* [1994] has shown that the zero potential vorticity flow in a rectangular channel has the greatest volume flux of all possible potential vorticity distributions. This is valid for all bottom shapes and makes the calculation of maximum fluxes easier than before. Earlier, *Killworth and McDonald* [1993] had found a maximum bound on any flow with nonnegative potential vorticity and showed it to be roughly the same as the zero potential vorticity relation.

3. OCEANIC OBSERVATIONS OF SILL FLOWS

We define sill as the deepest saddle point between neighboring deep basins. Numerous measurements or estimates of velocity in the vicinity of sills have been made, many of which are listed in Table 2. Table 2 is not an exhaustive list, but it contains a collection of studies with data that either give volume flux measurements or contain measurements from which such estimates can be obtained. The location of a number of these are shown in the three maps in Figure 5. The magnitude of volume flux varies from about 10^{-2} Sv to well over 1, depending upon the size of the basin. Most exhibit clear cross-channel tilt, a sign of influence of Earth rotation. Indeed, geostrophic estimates have been made of the speeds of many currents in such regions.

Four of the examples listed in Table 2 will be compared with an estimate from the idealized theory from section 2. To make this comparison, a methodology to estimate volume flux [*Whitehead*, 1989] will be used. The method requires only four numbers, the value of $\Delta\rho/\rho$, upstream height over the sill, channel width L, and the local Coriolis parameter. With these four parameters, volume flux can be predicted using either equation (12) or (13), which we repeat here for convenience:

$$Q = \frac{g' h_u^2}{2f} \qquad L > \left(\frac{2g' h_u}{f^2}\right)^{1/2}$$

$$Q = (\tfrac{2}{3})^{3/2} L \sqrt{g'} \left[h_u - \frac{f^2 L^2}{8g'} \right]^{3/2} \qquad \text{otherwise}$$

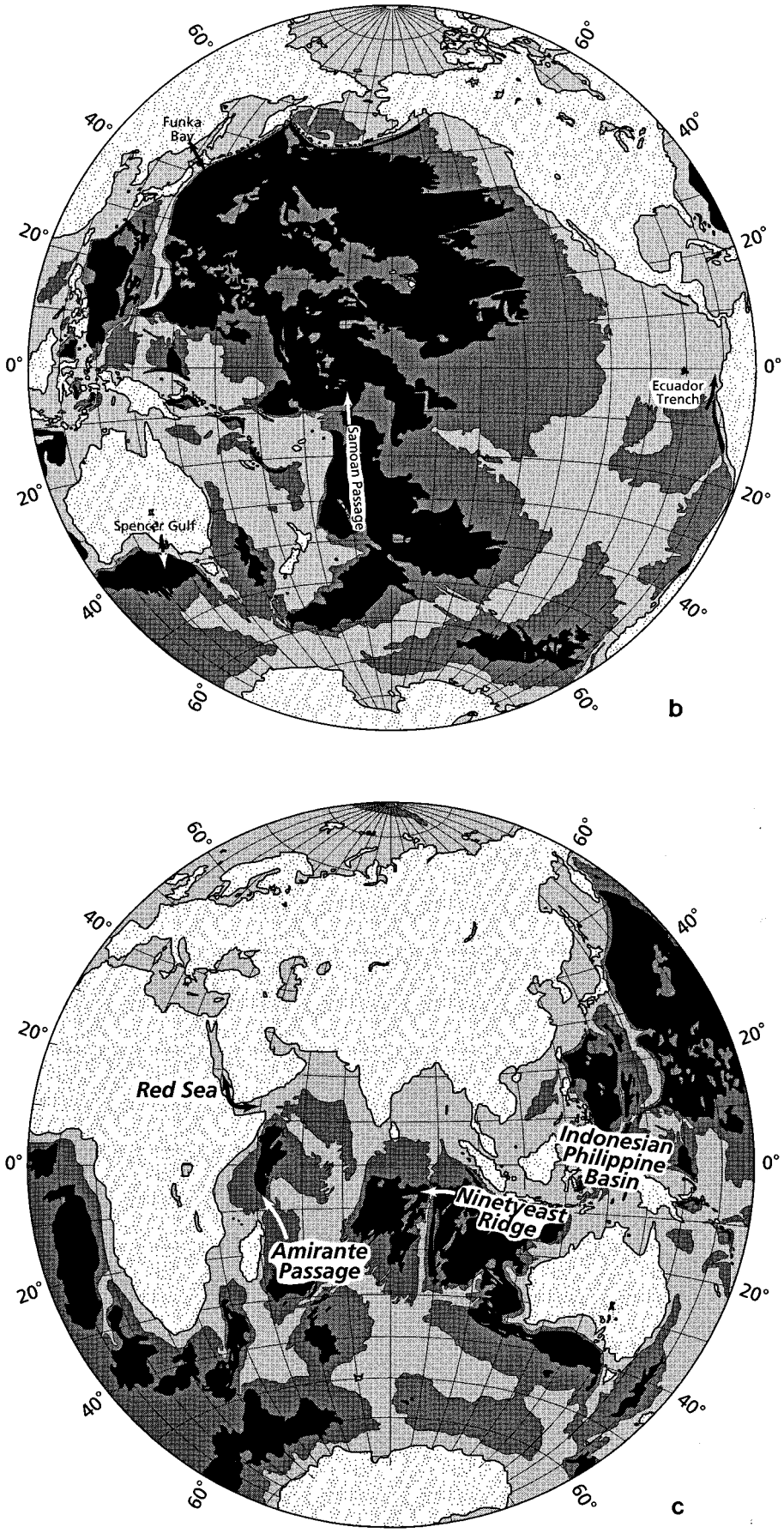

Figure 5. (continued)

To explain the method of obtaining the data required to produce a prediction from theory that can be compared with data, we use a sketch of the relevant features needed to estimate volume flux through a sill (Figure 6). The top section of this figure (plan view) shows a schematic top bathymetric view of a sill region, with deepest bathymetry darkest and shallower regions progressively lighter. A prominent topological feature of a sill region is the saddle point (S), which separates two unconnected deep basins (black). There are innumerable such saddle points in real bathymetry. Note, however, that this point also separates two shallower ridges (lightly stippled). If these extend around and surround the upstream basin above that saddle point depth, then that sill is the deepest connection for the dense deep water at sill depth between the two basins. Experience has shown that flow of deep water between the two basins will most likely be found in the vicinity of that saddle point. There is one depth whose contours (thick black lines) intersect at S. The depth of S is to be called the "sill depth," and in many cases it is even a "controlling" sill depth in the following sense. An elevation (side) view along a path leading from one deep basin to the other typically reveals relatively flat density surfaces above a fixed depth but a distinct departure from flatness in one of the two basins below a certain depth. Let us assume that deep, dense water has a source in one basin and is flowing over the sill into the other basin, which it partially fills but in which it also gets diluted with overlying water through turbulent mixing. We thus label two stations located on either side of S as U for upstream and D for downstream. This difference from flatness begins at the level where the two density versus depth curves taken at U and D split apart, or bifurcate, as shown on the right. We call this depth the "bifurcation depth." The upstream region (U) contains denser fluid below the bifurcation depth than downstream (D) since U contains undiluted deep water below sill depth and D contains deep water mixed with less dense overlying water.

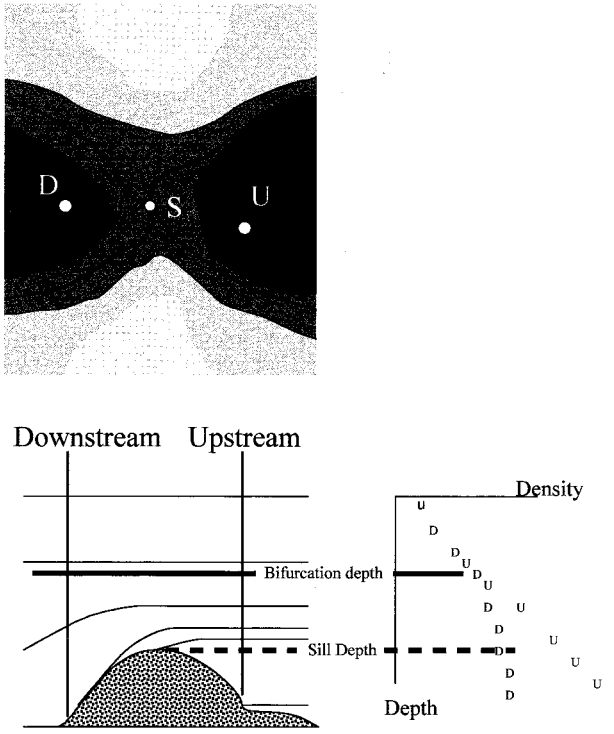

Figure 6. Map view sketch of a typical saddle point region (top). The darkest regions are deepest, and progressively lighter regions are shallower. One isobath connects between the two basins and the connection point defines a saddle point. A vertical section from one basin to the other (bottom, left) typically has asymmetry of density contours below a fixed depth but none above sill depth. We denote the basin with denser water as "upstream" (U) and the other "downstream" (D). On the bottom right the bifurcation depth between U and D, the sill depth definition, and consequent value of $\Delta\rho$ is shown.

To estimate $\Delta\rho/\rho$, we will select at least two density profiles from conductivity-temperature-depth (CTD) or bottle data, one upstream and one downstream of the sill that correspond to U and D in our sketch. The profiles must extend to the depth of the sill. The greatest density difference between upstream and downstream at or above sill depth will be used for the value of $\Delta\rho$. The sill depth is found from bathymetric charts. The bifurcation depth is subtracted from the sill depth to determine h_u. The width of the opening at the bifurcation depth will be used to determine L, and this width is determined through the use of bathymetric charts. Then either (12) or (13) will be used to calculate volume flux.

Such a method was used [*Whitehead*, 1989] to predict a volume flux using either equation (12) or (13) at four oceanic sills: the Denmark Strait, the ridge between Iceland and the Faeroe Islands, the Ceara Abyssal Plain, and the Vema Channel. These topographic control predictions were compared to flow estimates using current meter data for flow through three of the four passages. The second has only very indirect estimates of volume flux. It was erroneously compared to geostrophic estimates by *Steele et al.* [1962] downstream of the Iceland-Faeroe ridge which should include overflows from the Faeroe-Scotland ridge as well as the Iceland-Faeroe overflow. Therefore this second estimate will not be repeated.

The predictions of volume flux were all greater than the direct measurements, with ratios ranging from 1.6 to 4.1. While the smallest value of disagreement (60%) is understandable in view of the many assumptions contained in the comparison, the largest value (310%) is disturbingly large and may imply that the predictions are based on the wrong dynamics. We must keep in mind that both predictions and measurements have inherent errors from lack of resolution, and the source of disagreement was not clear at that time. Since 1989 it has been found that a substantial portion lies in errors of volume flux from the ocean measurements because more accurate measurements have been made. The new values and the ratio of prediction to measurements are

TABLE 3. Data and Predictions for Eight Sills

Sill	$\Delta\rho/\rho$, $\times 10^4$	h_w, *m*	f, $10^4\ s^{-1}$	L, *km*	R, *km*	Q, *Sv*	Q_{obs}, *Sv*	*Ratio* Q/Q_{obs}	*Reference*
Denmark Strait	3	580	1.3	350	14	3.8	2.9	1.3	*Dickson et al.* [1990]
Ceara Abyssal Plain	0.5	430	0.1	700	65	4.6	2.0	2.3	*Hall et al.* [1997]
Vema Channel	1	1540	0.7	446	25	16.3	6	2.7	*Speer and Zenk* [1993]
Discovery Gap	0.1	600	0.87	80	4	0.21	0.21	1	*Saunders* [1987]
Samoa Passage	0.3	1050	0.23	240	34	7.0	6	1.2	*Rudnick* [1997]
Vema Gap	0.5	1000	0.28	9	35	3.3	2.1	1.6	*McCartney et al.* [1991]
Faeroe Bank Channel	5	400	1.3	20	15	3.0	1.9	1.6	*Saunders* [1990]
Romanche Fracture Zone	0.47	380	0.02	20	369	2.2	1	2.2	*Polzin et al.* [1996]

shown in Table 3. The Iceland-Faeroe ridge flux estimates are excluded because no good estimates exist of the flux owing to errors explained above. The ratios are reduced to the range 1.3–2.7 by the better measurements, so disagreement ranges from 30 to 170%. This more agreeable range implies that the topographic control formulas are useful predictions of volume flux through deep ocean passageways. More important is the indication that the topographic control is the correct dynamics. As stated earlier, the zero potential vorticity calculations are known to predict larger flux than all others. Undoubtedly frictional and turbulent mixing effects also make a true flux smaller than predicted. In addition, the rectangular bottom geometry predicts higher flux than any other geometry. The magnitude of each of these effects has yet to be quantified for sill flows, although *Johnson and Ohlsen* [1994] make some estimates for exchange flows. Since the mid-1980s, measurements of volume flux have been made at a number of additional passageways, and these can also be compared with topographic control predictions. Thus here we extend this test of the topographic control method of predicting volume flux to five more cases, which are discussed in turn.

The first is Discovery Gap, a sill at a depth of approximately 4600 m that blocks Antarctic Bottom Water in its northward migration in the eastern North Atlantic. This sill connects the Madiera Abyssal Plain west of North Africa with the Iberian Abyssal Plain west of Portugal and Spain. *Saunders* [1987] used a variety of measurements to estimate volume flux through Discovery Gap, including yearlong measurements from six moorings and ten current meters, float-tracking data, and density profiles. A persistent current from southwest to northeast was found, both upstream (from the southwest) and over the gap. A detailed estimate of flux through various cross sectional areas over the gap produced an estimate of 0.21 ± 0.04 Sv of water colder than 2.05°C potential temperature.

Information for our prediction is contained in the bathymetry shown in Figure 7a and a bifurcation diagram of density distribution with depth at U and D is shown in Figure 7b. To obtain the latter, data for U had to be carefully selected since there was variation along the section shown by *Saunders* [1987, Figure 3]. Upstream conditions were complicated by an unmistakable

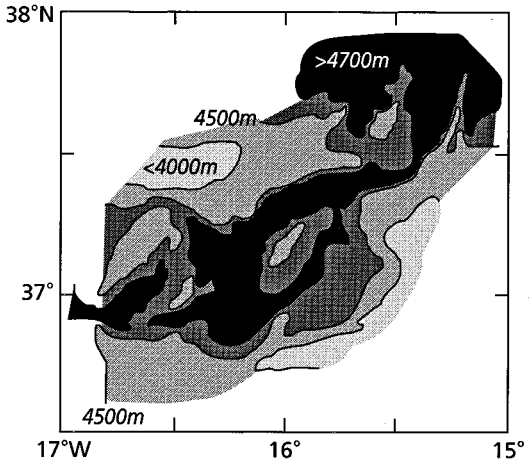

Figure 7a. Map showing the 4000-m, 4500-m, and 4700-m contours in the vicinity of Discovery Gap.

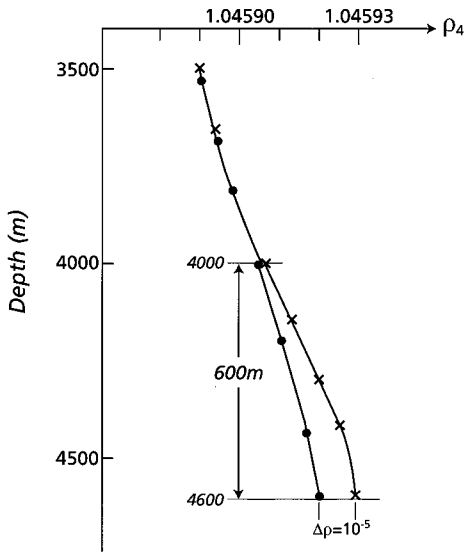

Figure 7b. Bifurcation diagram showing density (corrected to 4000 m) versus depth upstream and downstream of Discovery Gap.

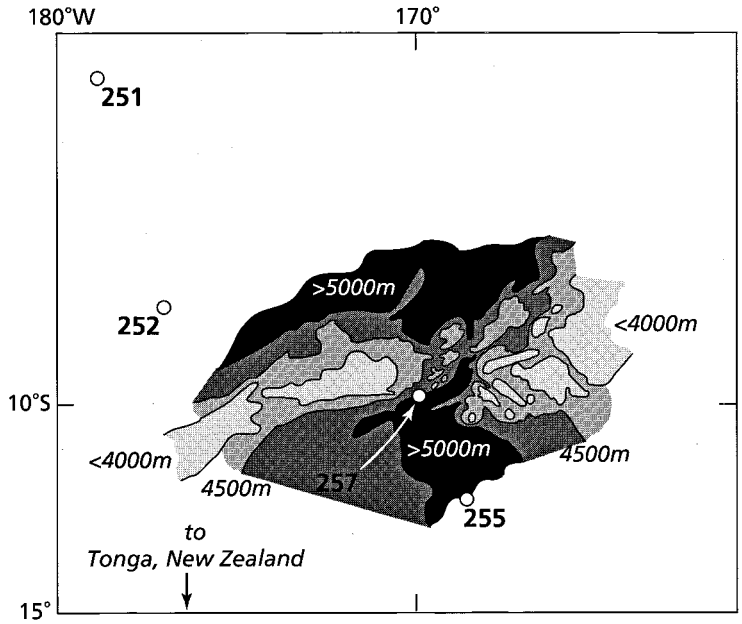

Figure 8a. Map showing the 4000-m, 4500-m, and 5000-m bottom contours near the Samoan Passage. Locations of the four Geochemical Ocean Sections Study (GEOSECS) stations are also shown.

cross stream tilt that signified a current of unknown origin. The final choice of data for U were selected from the station that represents the most reasonable upstream condition likely to affect the sill flow. From Figure 7b, the bifurcation depth was taken to be 4000 m. The reported shallowest sill depth was close to 4600 m, so

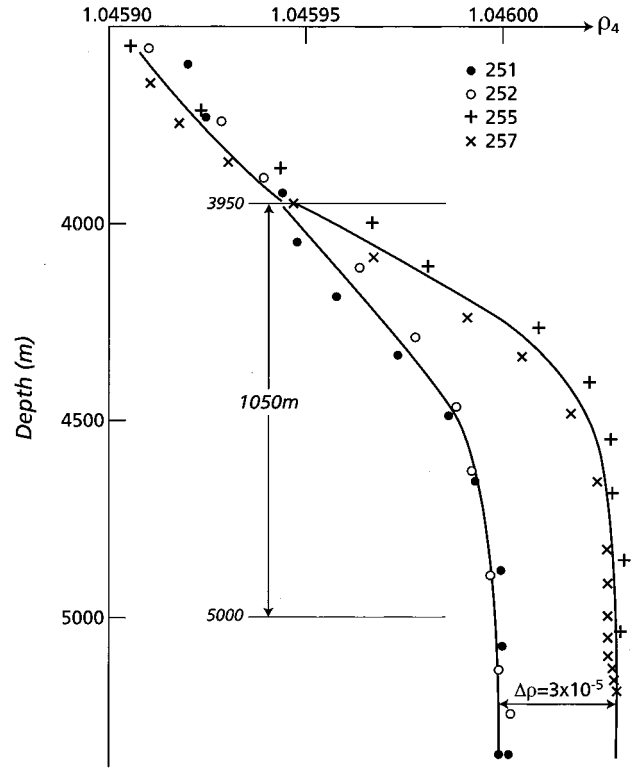

Figure 8b. Density (corrected to 4000 m) versus depth for the four GEOSECS stations upstream and downstream of the Samoan Passage.

$h_u = 600$ m and $\Delta\rho$ was taken to be 10^{-5} g cm^{-3}. Using $f = 0.87 \times 10^{-4}$ s^{-1}, which corresponds to the entrance sill at 36°54′N, this produces a Rossby radius $R = 4$ km, whereas the gap width is about 80 km for the 4000-m contour. Therefore the rapidly rotating formula equation (12) is used. It predicts volume flux of 0.2 Sv, which is extremely close to the measured value of 0.21 Sv. However, this very close agreement is clearly accidental, since there is an unusual amount of room for adjustment of this value. For example, the upstream density distribution varied from spot to spot. Second, the bathymetry is quite complicated. In fact, extreme values would predict volume flux down to half the value or up to 3 times bigger than the value.

The second flow is found through the deep Samoan Passage, the deepest saddle point–type passageway for the flow of Antarctic Bottom Water from the South to North Pacific. It consists (Figure 8a) of a channel with very complicated sidewalls that extends from about 11°S to about 9°S. Although flux estimates have been made in the past [*Reid and Lonsdale*, 1974] a recent current meter array produced a comprehensive long term data set [*Rudnick*, 1997] for a more complete estimate of 6 Sv. Our data (Figure 8b) are taken from Geochemical Ocean Sections Study (GEOSECS) Pacific stations 251 and 252 (upstream) and 253 and 257 (downstream). This gives a bifurcation depth of 3950 m. The bathymetric map, traced from the GEBCO map, shows a width of 240 km at this depth. Rudnick shows a sill depth in excess of 4800 m; assigning a maximum value of 5000 m, we find $h_u = 1050$ m and $\Delta\rho/\rho = 3 \times 10^{-5}$. The Rossby radius computed from these numbers and using the Coriolis parameter for 9°S of $f = 0.23 \times 10^{-4}$ s^{-1} is $R = 34$ km, so the rapid rotating limit should be used.

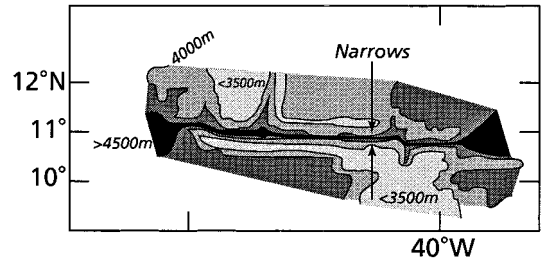

Figure 9a. Map showing the 3500-m, 4000-m, and 4500-m contours near the Vema Gap.

This gives $Q = 7.0$ Sv, which is very close to the estimate of 6 Sv based on current meter data.

The third example is the Vema Gap (Figures 9a and 9b). This gap lies at about 11°N in the Mid-Atlantic Ridge. Historically, the source of the Antarctic Bottom Water in the tropical Eastern Atlantic was considered to be a flow through the Romanche Fracture Zone that lies almost exactly on the equator. However, the work of *Vangriesheim* [1980] and *Eittreim et al.* [1983] indicated that the flow through the Vema Fracture Zone was a major contributor to the water in the eastern North Atlantic. Recently, *McCartney et al.* [1991] estimated a flux of 2.1–2.3 Sv through the Vema Gap using geostrophic calculations. The data for this example are shown in Figure 8b. From it we take $h_u = 1000$ m, $\Delta\rho/\rho = 0.5 \times 10^{-4}$, which, along with $f = 2.8 \times 10^{-5}$ s^{-1} (for 11°N) and $g = 9.8$ m s^{-2}, predicts a Rossby radius of 35 km. This is wider than the passage width $L = 9$ km, so equation (13) is used to predict volume flux. With the numbers given above, this comes out to be 3.3 Sv. This is about 50% over the observed geostrophic estimate (which was estimated downstream of the sill, where turbulence and presumably strong entrainment of ambient water have been seen elsewhere [*Polzin et al.*, 1996]). Corrections to the hydraulic estimate could be made by accounting for the tapering of the walls of the gap, for the influence of continuous stratification, and possibly for friction [*Pratt*, 1986].

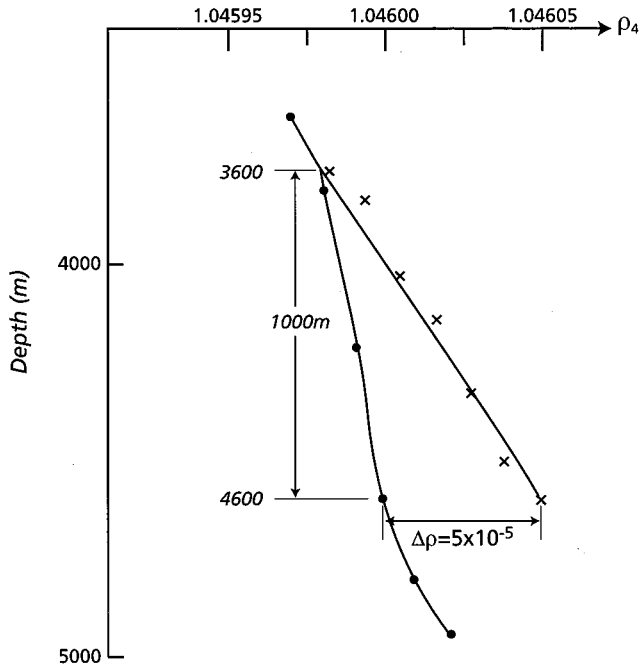

Figure 9b. Density (corrected to 4000 m) versus depth for selected stations upstream and downstream of Vema Gap.

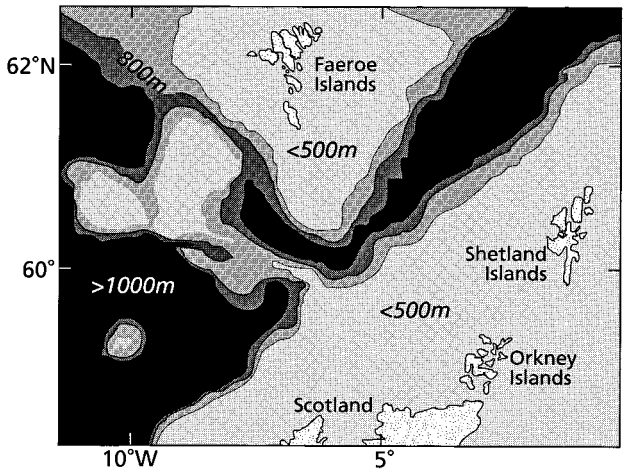

Figure 10a. Map showing the 500-m, 800-m, and 1000-m contours near the Iceland-Faeroe passage dense surface water. Obviously, a large number of stations have dense water above the selected bifurcation depth. Such dense shallow water does not reach the strait.

The fourth example is the Faeroe Bank Channel (Figure 10a). Dense water from the Norwegian Sea flows southward between the Faeroe and Shetland Islands. It then veers toward the west and flows along the Faeroe Bank Channel, which extends between the Faeroe Islands and the Faeroe Banks. This channel has a saddle point depth of about 900 m at about 61°N. The bifurcation diagram Figure 10b is made using 2880 stations from the National Oceanographic Data Center (NODC) data atlas. Stations with the deepest bifurcation have a bifurcation depth of 500 m. Nearby station pairs that are closer to the shelf have significantly shallower bifurca-

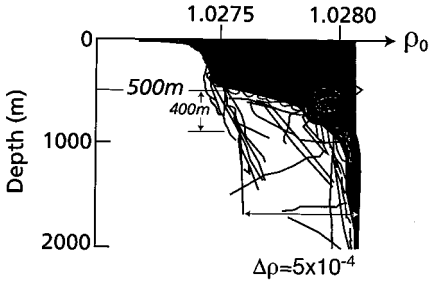

Figure 10b. Density versus depth for 2880 stations upstream and downstream of the Iceland-Faeroe passage. Obviously a large number of stations have dense water above the selected bifurcation depth. Such dense water does not reach the strait.

tion depth due to fresh water over the shelf. The sill depth is reported to be 900 m, which gives $\Delta\rho/\rho = 5 \times 10^{-4}$. Using $f = 1.3 \times 10^{-4}$ s^{-1}, we obtain $R = 15$ km. Using $L = 20$ km, the rapid rotation limit is used. The prediction of volume flux using equation (12) is 3 Sv, whereas *Saunders* [1990] reports 1.9 Sv. *Borenäs and Lundberg* [1988] used a parabolic bottom and selected the 3°C isotherm and got good agreement with Saunders' measurement. *Johnson and Ohlsen* [1992] show velocity and density evidence of a strong, frictionally driven secondary circulation. This could also be responsible for a lower observed transport than theory.

The last estimate is for flux of Antarctic Bottom Water through the Romanche Fracture Zone, in which two sills and a narrows produce a complicated control geometry at the western end. The prediction of flux using hydraulic control was done by *Mercier and Bryden* [1994] using the traditional maximized flow formula (equation (13) with $f = 0$) to produce an estimate of 2.4 Sv. Their method is identical to that used here except that they estimated density difference by subtracting the density of the water with average temperature (and salinity) of the transition layer, which they defined as the layer above sill depth, from the density of water with temperature that defines the top of that layer. The average temperature of the transition layer was put to $\theta = 1.55$°C and the top of the layer was set to $\theta = 2.0$°C, with a density difference between the two waters of 4.7×10^{-5} g cm^{-3}. Our method produces somewhat different values. Figure 11 is a bifurcation diagram produced directly from their potential temperature section [*Mercier and Bryden*, 1994, Figure 1] along the axis of the Romanche Fracture Zone. Upstream was taken as the most western point and downstream the most eastern point. The sill depth of 4350 was given by them; it results in a temperature difference of 0.7°C in contrast to their value of 0.45, so we take a proportionate density difference of 7.3×10^{-5} g cm^{-3}. The depth of the top of the layer is more difficult to assign. Our bifurcation diagram has a kink just below the depth of bifurcation, which indicates two choices for the depth of the top of the water layer. In one case the two temperatures come together at 3750 m; in the other the upstream properties linearly extrapolate to the downstream properties at a much greater depth of 3970 m. In both cases the Rossby radius of deformation is absurdly huge, 463 and 369 km compared with the 20-km estimated width of the passage, so that rotation is unimportant. Thus we take the weakly rotating formula equation (13), but use the deep value to get $h_u = 380$ m, with a consequent estimate of 2.2 Sv. This flux estimate is close to the value found by Mercier and Bryden, although they selected a smaller value of density difference and a larger top depth (midway between our two values). A measurement of 1 Sv based on one set of current profiles is reported by *Polzin et al*. [1995]. There is no information about probable time variations in the strength of the current at present.

All the values of the assorted parameters are shown in Table 3. Three data sets are updated from *Whitehead* [1989], and five are new ones discussed here. The observed flux is also plotted against predicted flux in Figure 12. Logarithmic scales are used to compare data over a range of almost 2 orders of magnitude. A linear comparison would be useless. It is clear that the predictions are of the same order as the measured values but generally are greater. Indeed, the ratio of predicted to observed flux has the reasonable range of 1.0 to 2.70. However, the method still must be used with caution if additional currents are present; otherwise, the prediction has unrealistically great values of h_u, and flux is greatly overpredicted. The present prediction has considerable uncertainty from shortcomings of available data. The four parameters f, h_u, $\Delta\rho/\rho$, and L are used to predict flux, and uncertainty in each contributes uncertainty to the flux prediction. The value of h_u seems to be the most important in producing uncertainty in flux. This arises for three reasons. First, bifurcation depth is typically determined from only a few CTD casts, so that scatter from currents, eddies, and even distance from the sill region produces variation of up to 100 m or more from what is expected to be a true long-term value. Second, sill depth is uncertain in most bathymetric data sets by up to 100 m. Third, h_u is raised to a power greater than 1.

4. STRAIT FLOW CALCULATIONS: LOCK EXCHANGE THEORY

The previous sections discussed the case where the sill lies at some depth in a large ocean within which are small deep basins whose boundaries are defined by subsurface ridges. Such ridges usually arise from mid-ocean ridges, hotspots, or other anomalous features, but there are also shallower sills in basins bordered by continental material. If a saddle point lies in a passage whose sidewalls (lightly stippled in Figure 6) extend to the surface of the ocean, and if those surface ridges surround the upstream basin above sea level, the flow in the passage is usually found to be an exchange flow that has currents with roughly the same flux of water in both directions.

The saddle point is usually proximal to straits. The bidirectional flow we will call lock-exchange flow. The flow itself arises because the basins contain water of different surface densities from temperature and salinity difference.

In formulating this kind of problem, one could picture a gate that, once removed, allows the setup of a semisteady exchange of flow and counterflow between the basins. Predictions for the strength of such flow in the absence of the effects of fluid rotation are well known. Formulas are found in numerous textbooks of hydraulics [e.g., *Yih*, 1980]. However, the effects of Earth rotation may be felt in such problems in the ocean. This problem with rotation included was analyzed for zero potential vorticity by *Whitehead et al*. [1974]. In that formulation a

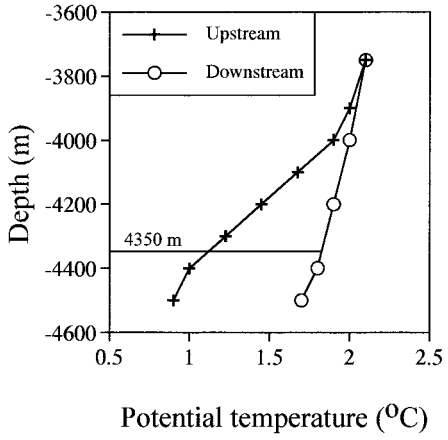

Figure 11. Potential temperature versus depth upstream and downstream of the Romanche Fracture Zone.

somewhat questionable energy-conserving formula applicable to flow in a channel with a level bottom was used in conjunction with zero potential vorticity, which requires very deep upstream regions. Although laboratory data agreed with the theoretical prediction, a more complete theory would be useful. *Dalziel* [1988, 1990] extended the formalism introduced by *Gill* [1977] from one layer flow to two layers with opposing flows. A number of improvements were obtained for openings less than one Rossby radius in width. An improvement for wide channels was later made by *Hunkins and Whitehead* [1992] as reviewed here. The model (Figure 13) consisted of two basins separated by a channel of depth H. Basin 1 has water of density ρ_1, and basin 2 has water of greater density. We solve inviscid, nondiffusive, two-layer flow.

One geometrical constraint for the flow in the channel is conservation of depth,

$$h_1(x) + h_2(x) = H \tag{16}$$

where h_1 and h_2 are vertical thickness of each layer of water in the strait, shown in Figure 13, with subscript 1 denoting the top layer. We have assumed that deflection of the sea surface is negligible. A second equation is conservation of potential vorticity for each layer

$$\frac{\partial v_1}{\partial x} + f = \frac{fh_1}{H} \tag{17}$$

$$\frac{\partial v_2}{\partial x} + f = \frac{fh_2}{H} \tag{18}$$

and a third is thermal wind between the two layers.

$$f(v_2 - v_1) = g' \frac{\partial h_2}{\partial x} \tag{19}$$

where g' is reduced gravity from density difference between the two fluids as used in the preceding sections. One can derive differential equations for h_1, h_2, v_1, and v_2 as follows:

Take the x derivative of (19) and use (17) and (18) to get

$$\frac{\partial^2 h_2}{\partial x^2} - \frac{f^2}{g'}\left(\frac{2}{H}\right)h_2 = -\frac{f^2}{g'} \tag{20}$$

It is convenient to define x as being zero in the middle of the channel. The solution of h_2 is

$$h_2 = \frac{H}{2} + B \cosh\frac{x}{R} + A \sinh\frac{x}{R} \tag{21}$$

and from (16), the solution of h_1 is

$$h_1 = \frac{H}{2} - B \cosh\frac{x}{R} - A \sinh\frac{x}{R} \tag{22}$$

where $R = \sqrt{g'H/2f^2}$ and A and B are constants of integration. To solve for velocity, use (17) and integrate:

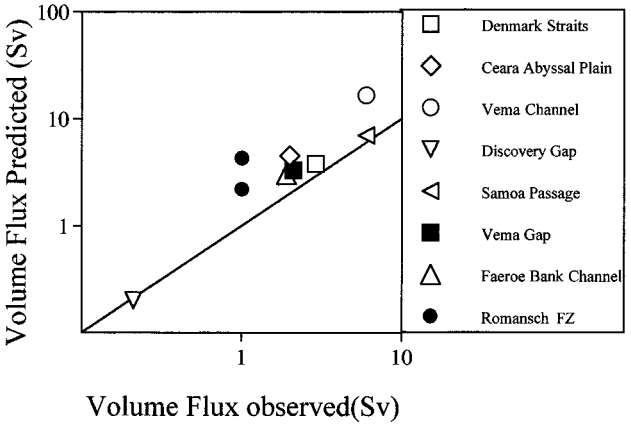

Figure 12. Predicted values of volume flux compared with observed values as listed in Table 3. The predictions for the Vema Gap and the Romanche Fracture Zone (solid symbols) are the only ones using the weakly rotating hydraulics equation (12); the rest use (13). The line has slope of unity.

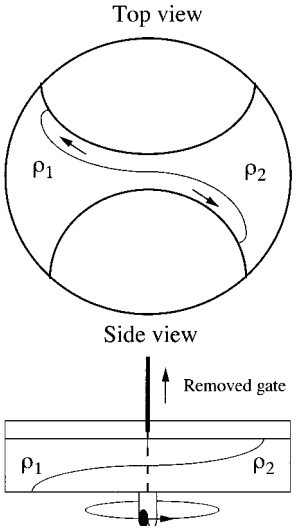

Figure 13. Sketch of a lock-exchange flow through a long, straight channel.

$$v_1 = -\frac{fx}{2} - \frac{fRB}{H}\sinh\frac{x}{R} - \frac{fRA}{H}\cosh\frac{x}{R} + C \tag{23}$$

or use (18) and integrate:

$$v_2 = -\frac{fx}{2} + \frac{fRB}{H}\sinh\frac{x}{R} + \frac{fRA}{H}\cosh\frac{x}{R} + D \tag{24}$$

Here C and D are also constants of integration.

These constants are found as follows: First, equation (19) dictates that $C = D$. Second, it is easy to show that the antisymmetric profile gives maximum flux, all others things being fixed. Assume that the height profile is antisymmetric about the horizontal centerline of the tank, so that $B = 0$. Given antisymmetry of the profile, the assumption of equal and opposite volume flux through the strait requires that $v_1 = -v_2$ at $x = 0$. This requires that $C = 0$, so only the constant A remains to be determined.

Gill [1977] showed that the constant potential vorticity current has a Bernoulli function that is easily determined except for a constant. Since there is no dissipation in the current, the constant is conserved along streamlines. Therefore the antisymmetric solution for the current extends throughout the entire region from behind one nose through the passage to behind the other nose.

To solve for the final constant, the time-dependent energy equation was used. It has the form

$$\frac{\rho}{2}\frac{\partial\langle v^2\rangle}{\partial t} + g'\langle w\Delta\rho\rangle = 0 \tag{25}$$

where only the deviation of density $\Delta\rho$ from a constant value ρ has been retained and w is vertical velocity. The angle brackets denote a volume integral over the entire current, including the noses.

We do not know the detailed flow in the nose region, but we picture a situation like that in Figure 13, so the nose is fully developed (see *Stern* [1980], *Stern et al.* [1982], and *Griffiths and Hopfinger* [1983] for studies of the noses of rotating bores). Hence it will be self-similar between a time t and a time $t + \delta t$. The similarity assumption requires that the volume of the moving nose region be unchanging, in which case we can set nose speed $c_i = Q_i/A_i$, where Q_i is the magnitude of the volume flux of the ith current behind the nose and A_i is the cross-sectional area of the current.

Thus the increase in internal kinetic energy in time equals c_i times the cross section areal average of kinetic energy across the current. These are summed for the two on the left and the two on the right to give

$$\rho\frac{\partial\langle v^2\rangle}{\partial t} = \frac{\rho}{2}\left(\frac{Q_1}{A_1} + \frac{Q_2}{A_2}\right)\left(\int_{-\lambda/2}^{\lambda/2} v_2^2 h_2\,dx + \int_{-\lambda/2}^{\lambda/2} v_1^2 h_1\,dx\right) \tag{26}$$

Likewise, the increase in potential energy is equal to c_i times the area of the current times the vertical displacement of the center of gravity of each column of width dx. The product of these is integrated across the currents and summed for the two noses to give

$$g\langle w\Delta\rho\rangle = \frac{Q_2}{A_2}\int_{-\lambda/2}^{\lambda/2} g\Delta\rho\,\frac{h_2^2}{2}\,dx - \frac{Q_1}{A_1}\int_{-\lambda/2}^{\lambda/2} g\Delta\rho h_1\left(\frac{h_1}{2} + h_2\right)dx \tag{27}$$

Equations (26) and (27) are set equal, and since $Q_1 = Q_2$, $h_1 = H - h_2$, and $A_1 = A_2$, they simplify to

$$\frac{\lambda^3}{24R^3} + \frac{A^2}{H^2}\left(\frac{\lambda}{R}\left(1 - \cosh\frac{\lambda}{R}\right) + 4\sinh\frac{\lambda}{R}\right) = \frac{\lambda}{R}\left(1 + \frac{2A^2}{H^2}\right) \tag{28}$$

where

$$A\sinh\frac{\lambda}{2R} = \frac{H}{2} \tag{29}$$

These two equations are satisfied for the values

$$\lambda/2R = 2.5940 \qquad A/H = 0.07514 \tag{30}$$

Since A was the last remaining unknown, volume flux can now be determined from the integral

$$Q_1 = Q_2 = \int_{-\lambda/2}^{\lambda/2} h_1 v_1\,dx = fAR\left(\frac{\lambda}{2}\cosh\frac{\lambda}{2R} - 2\sinh\frac{\lambda}{2R}\right) = 0.156\,\frac{g'H^2}{f} \tag{31}$$

Whitehead et al. [1974] used the flat bottom energetics shown above with the admittedly incorrect zero potential vorticity velocity profile to predict $Q_1 = g'H^2/6f$ which is 7% higher. This is consistent with the notion that the zero potential vorticity flux is an upper bound. Unfortunately this has not yet been shown to be true for the lock-exchange case as Killworth has shown for a sill. This volume flux prediction has been checked by a laboratory experiment by *Hunkins and Whitehead* [1992]. Both the slope and the constant in front agree with the data to better than 10%.

5. OCEANIC ESTIMATES OF EXCHANGE FLOWS

Lock-exchange calculations similar to (31) have now been used in numerous ocean applications; some examples are the Strait of Gibraltar, Spencer Gulf, Chesapeake Bay, Delaware Bay, and Funka Bay (Uchiura Wan). Table 4 contains a list of such straits for which at least partial information of flux through the opening is

TABLE 4. Flux and Density Difference Estimates for Some Oceanic Strait Flows

Strait	*FW Flux, $m^3\ s^{-1}$*	*H, m*	*f, $s^{-1} \times 10^4$*	*L, km*	*R, km*	*$\Delta\rho/\rho \times 10^4$*	*Q, Sv*	*$(\Delta\rho/\rho)/obs \times 10^4$*	*Reference*
Strait of Gibraltar		300	1.0	12	20	2	0.8	3	*Whitehead et al.* [1974], *Bryden and Stommel* [1984]
Spencer Gulf	−200	40	0.8	50	3.2	6.8	0.02	9	*Bye and Whitehead* [1975]
Chesapeake Bay	2237	10	0.9	19	4	50	0.01	65	*Whitehead* [1989]
Funka Bay (Uchiura Wan)	···*	80	1.0	21	3.9	···*	0.03	7	*Miyake et al.* [1988]
Fram Strait	10^4	200	1.4	>200	5.0	7	0.3	7	*Hunkins and Whitehead* [1992]
Baltic entrance	14,000	18	1.2	100	6.2	60	0.03	70	this study

Other strait flows include the following: Delaware Bay, Bab el Mandab, Suez Canal, Strait of Juan de Fuca, Strait of Tiran, Skagerrak, Adriatic shelf break, Bass Strait, Strait of Belle Isle, Gulf of Mexico, Tsugaru Strait, and Bosporus.

*This information was not used for this study.

given. Here we use these formulas for the connecting passage between the Baltic and the North Sea.

In the Baltic, *Petren and Walin* [1976] measured the flow of salty bottom water into the Baltic through the Bornholm Strait during the period of June 1973 to December 1974. They used geostrophic calculations and gel current meters to estimate that the bottom salty water volume flux was somewhere between 11,500 and 17,200 $m^3\ s^{-1}$, depending upon the limiting salinity used, which ranged from 8.25 to 9.575‰, and upon the method of averaging. The volume flux estimate was used along with salt conservation considerations of the outflow of surface water with salinity of 8‰ to estimate how much river inflow would be needed for a salt flux of zero. They calculated a fresh water discharge of 9400 to 12,000 $m^3\ s^{-1}$ which is reasonably close to the measured mean fresh water supply to the Baltic, which averaged 14,000 $m^3\ s^{-1}$ for the period 1951–1970. Their reason for measuring the flux of deep water through the Bornholm Strait was that such flows are steadier than the flows in the entrance regions. For instance, the Baltic has a narrow, shallow (~18 m) entrance region, and currents in the region are variable because of variations in surface level. Such variations make measurements difficult unless taken for very long periods of time. We can, however, use a lock-exchange estimate using the considerations stated by *Bye and Whitehead* [1975] to predict the salinity difference between the deep and shallow water in the Baltic. This will assume that salinity difference is controlled by exchange flow in the Baltic entrance, in response to the mean fresh water supply of 14,000 $m^3\ s^{-1}$. In this the balances of volume flux Q and salt flux are

$$Q_i + Q_r + Q_o = 0 \tag{32}$$

$$S_iQ_i = S_oQ_o \tag{33}$$

where subscripts i, o, and r stand for "into the Baltic," "out of the Baltic," and "from river inflow," respectively. In this we assume that Q_r and S_i are fixed by climatological factors and specified, whereas the other quantities can vary. Equations (32) and (33) can be combined to give

$$Q_o\Delta S = S_iQ_r \tag{34}$$

where $\Delta S = S_i - S_o$. A dynamic condition relating the volume flux to the density difference between inflowing and outflowing water in a shallow sill region is

$$Q_o = \frac{g\Delta\rho H^2}{6\rho f} = \frac{g\beta\Delta S H^2}{6f} \tag{35}$$

where $\beta = 0.7 \times 10^{-3}(‰)^{-1}$ is the coefficient of density change due to change in salinity, H is depth of the sill, and $f = 1.2 \times 10^{-4}\ s^{-1}$ is the Coriolis parameter for 55°N. This formula applies to steady flow in a flat channel of both length and width greater than Rossby radius (to be calculated post facto), and it is assumed that both $Q_o \approx Q_i$ and $S_o = S_i$. Equations (34) and (35) are combined to eliminate Q_o, and a salinity difference is predicted to be

$$\Delta S = \left(\frac{6fS_iQ_r}{g\beta H^2}\right)^{1/2} \tag{36}$$

Using $g = 9.8\ m\ s^{-1}$, $H = 18$ m, $S_i = 18‰$, $Q_r = 14{,}000\ m^3\ s^{-1}$, and the values given above for f, and β, the formula predicts salinity difference between outflow and inflow to be 9‰.

We next calculate volume flux from (37) as 27,800 $m^3\ s^{-1}$, which is close to the value of the outflows estimated by *Petren and Walin* [1976]. Since Q_r is roughly the same magnitude as Q_o, the assumption that $Q_o \approx Q_i$ is relatively poor. The present result is relatively insensitive to the value of salinity. If the salinity of the inflowing water with 8‰ was used, for example, we would predict a salinity difference about two thirds as large as the present prediction. In that case, the volume flux, which is linearly proportional to salinity difference, would also be two thirds of the present value. Finally, the Rossby radius of deformation can be calculated from the formula

$$R_o = \left(\frac{g\beta\Delta S H}{2f^2}\right)^{1/2} \tag{37}$$

and it is 6.2 km using the values given above.

The same technique has been used for a number of

other basins. These are listed in Table 4. The density difference is predicted along with a volume flux. The observed density difference is also presented; the value was obtained using data in the cited studies. The ratio of predicted to observed density difference ranges from 0.66 to 1. The fact that the ratio is less than 1 is consistent with the expectation that the idealized frictionless two-layer flow will predict a flux greater than the true value. The test is deliberately crude, but it is applied to a number of examples over a wide range of parameters, so that the suitability of the calculations can be assessed for future, more thorough studies.

6. CLOSING REMARKS

By employing the very simplest inertial theory and by deliberately using easily obtainable archival data, we indicate that to a crude first approximation, the simple control-flow formulas produce sensible estimates of interbasin flux. Our comparisons depend on having ocean estimates of flux through the opening. Fortunately, since flow through such constrictions is often concentrated, superior oceanographic estimates of flux, velocity, and time dependence can be made in such regions. This has attracted a sizable number of oceanographers to make measurements in such regions. Consequently, the number of comparisons has steadily risen from the three or four in the mid-1970s to over 20 now. Thus the range of parameters over which tests like these have been made is steadily increasing.

Along with the improvement in the ocean data, numerous theoretical advances have been made. Most of them concern assorted effects from variable potential vorticity. These effects include altered upstream flow patterns and control behavior. No significant effects upon volume flux have been reported by the variation of potential vorticity unless such variation produces very large upstream currents. A few studies have been made of the role of friction and time dependence. Two areas that need work but in which little or none has been done to date, are numerical modeling and effects of continuous stratification. Although this review focused on quiescent upstream conditions, wind setup can produce important effects to surface layers [*Nof and Olson*, 1983; *Nof*, 1995b].

The present predictions have considerable uncertainty resulting from shortcomings of the available data. As was mentioned before, the four parameters f, h_u, $\Delta\rho/\rho$, and L are used to predict flux, but uncertainty in each contributes uncertainty to the flux prediction. The value of h_u is produced from information of bifurcation depth, which is typically determined from a number of CTD casts, so that scatter from currents, eddies, and even distance from the sill region produces variation up to 100 m or more from what is expected to be a true long-term value. Second, sill depth is uncertain. Third, the result is sensitive to h_u raised to a power greater than 1. The resulting uncertainties in flux prediction are presently as large as the uncertainty of the direct estimate of flux from extensive current meter data sets. Finally, frictional effects should move the critical point to a region downstream of the sill, but how to determine the location of the critical point in detail is not yet understood.

In spite of these limitations to both prediction and measurements, results indicate that the control dynamics may play a role in the flow through the passageway (as is advocated here), since the parameters span a wide range of values. Thus additional precision can be achieved by including more realism such as continuous stratification, more realistic bathymetry, and friction. None have been completely included in either unidirectional or bidirectional controlled rotating flow problems yet, so understanding of this promising dynamics remains in its infancy despite more than 20 years of work.

In the ocean, we know almost nothing about the local aspects of such flows. What is the nature of a real upstream flow? How much does local topography influence the currents? Is there significant dynamic influence by nearby currents? Is friction enhanced by the concentrated currents, and if so, where? Is vertical mixing influenced near the control region, as it is downstream of the control point [*Polzin et al*., 1996]? Is vertical mixing enhanced in certain regions, such as on the left-hand side, where currents are greatest? Is side or bottom friction enhanced there? I hope that the answers to some of these questions will be found by future studies.

ACKNOWLEDGMENTS. Support for these studies have been received from the Office of Naval Research under grant N00014-97-1-0195. Woods Hole Oceanographic Institution contribution 9677.

D. Luther was the Editor responsible for this paper. He thanks K. Borenäs, D. Nof, and three anonymous reviewers for their assistance in evaluating the paper.

REFERENCES

Bethoux, J. P., Budgets of the Mediterranean Sea: Their dependence on the local climate and the characteristics of the Atlantic waters, *Oceanol. Acta*., *2*, 3, 157–163, 1979.

Borenäs, K., and P. Lundberg, Rotating hydraulics of flow in a parabolic channel, *J. Fluid Mech*., *167*, 309–326, 1986.

Borenäs, K. M., and P. A. Lundberg, On the deep-water flow through the Faeroe Bank Channel, *J. Geophys. Res*., *93*, 1281–1292, 1988.

Borenäs, K. M., and L. Pratt, On the use of rotating hydraulic models, *J. Phys. Oceanogr*., *24*, 108–123, 1994.

Bryden, H., and H. Stommel, Limiting processes that determine basic features of the circulation in the Mediterranean Sea, *Oceanol. Acta*, *7*(3), 289–296, 1984.

Bye, J. A. T., and J. A. Whitehead Jr., A theoretical model of the flow in the mouth of Spencer Gulf, South Australia, *Estuarine Coastal Mar. Sci*., *3*, 477–481, 1975.

Dalziel, S. B., Two-layer hydraulics: Maximal exchange flows, Ph.D. thesis, Univ. of Cambridge, Cambridge, England, 1988.

Dalziel, S. B., Rotating two-layer sill flows, in *Physical Oceanography of Sea Straits*, *NATO-ASI Ser*., *Ser. C*, vol. 318, edited by L. J. Pratt, pp. 343–371, Kluwer Acad., Norwell, Mass., 1990.

Dickson, R. R., and J. Brown, The production of North Atlantic Deep Water: Sources, rates and pathways, *J. Geophys. Res*., *99*, 12,319–12,341, 1994.

Dickson, R. R., E. M. Gmitrowicz, and A. J. Watson, Deep water renewal in the northern Atlantic, *Nature*, *344*, 848–850, 1990.

Ettreim, S. L., P. E. Biscaye, and S. S. Jacobs, Bottom water observations in the Vema Fracture Zone, *J. Geophys. Res*., *88*, 2609–2614, 1983.

Garrett, C. J. R., Variable sea level and strait flows in the Mediterranean: A theoretical study of the response to meteorological forcing, *Oceanol. Acta*, *6*, 79–87, 1983.

Garrett, C. J. R., and F. Majaess, Non-isostatic response of sea level to atmospheric pressure in the eastern Mediterranean, *J. Phys. Oceanogr*., *14*, 656–665, 1984.

Garrett, C. J. R., and B. Toulany, Sea level variability due to meteorological forcing in the northeast Gulf of St. Lawrence, *J. Geophys. Res*., *87*, 1968–1978, 1982.

Garzoli, S., and C. Maillard, Hydrologie et circulation hivarnales dans les canaux de Sicile et de Sardaigne, report, 21 pp., *Rapp. Int. Lab. Oceanogr. Phys. Mus. Natl. Histoire Nat*., Paris, 1976.

Gill, A. E., The hydraulics of rotating channel flow, *J. Fluid Mech*., *80*, 641–671, 1977.

Grancini, G. F., and A. Michelato, Current structure and variability in the Strait of Sicily and adjacent area, *Ann. Geophys*., *Ser. B*, *5*(1), 75–88, 1987.

Griffiths, R. W., and E. J. Hopfinger, Gravity current moving along a lateral boundary in a rotating fluid, *J. Fluid Mech*., *134*, 357–399, 1983.

Hall, M., M. McCartney, and J. A. Whitehead, Antarctic Bottom Water flux in the equatorial western Atlantic, *J. Phys. Oceanogr*., *27*, 1903–1926, 1997.

Hogg, N., P. Biscaye, W. Gardner, and W. J. Schmitz, On the transport and modification of Antarctic Bottom Water in the Vema Channel, *J. Marine Res*., *40*, suppl., 231–263, 1982.

Hunkins, K., and J. A. Whitehead, Laboratory simulation of exchange through Fram Strait, *J. Geophys. Res*., *97*, 11,299–11,321, 1992.

Johnson, G. C., and D. R. Ohlsen, Frictionally modified rotating hydraulic channel exchange and ocean outflows, *J. Phys. Oceanogr*., *24*, 66–78, 1994.

Johnson, G. C., D. L. Rudnick, and B. A. Taft, Bottom water variability in the Samoa Passage, *J. Mar. Res*., *52*, 177–196, 1994.

Killworth, P. D., Flow properties in rotating, stratified hydraulics, *J. Phys. Oceanogr*., *22*, 997–1017, 1992.

Killworth, P., On reduced-gravity flow through sills, *Geophys. Astrophys. Fluid Dyn*., *75*, 91–106, 1994.

Killworth, P. D., and N. R. McDonald, Maximal reduced-gravity flux in rotating hydraulics, *Geophys. Astrophys. Fluid Dyn*., *70*, 31–40, 1983.

Luyten, J. M., M. McCartney, H. Stommel, R. Dickson, and E. Gmitrowicz, *J. Phys. Oceanogr*., *23*, 1885–1892, 1993.

McCartney, M. S., and R. A. Curry, Trans-equatorial flow of Antarctic bottom water into the western Atlantic Ocean, *J. Phys. Oceanogr*., *23*, 1264–1276, 1993.

McCartney, M. S., S. L. Bennett, and M. E. Woodgate-Jones, Eastward flow through the Mid-Atlantic Ridge at 11°N and its influence on the abyss of the eastern basin, *J. Phys. Oceanogr*., *21*, 1089–1120, 1991.

Mercier, H., and H. Bryden, Flow of Antarctic Bottom Water over the sill in the Romanche Fracture Zone, *Int. WOCE Newsl*., *17*, pp. 9–10, WOCE Int. Proj. Off., Southampton, England, 1994.

Miyake, H., I. Tanka, and T. Murakami, Outflow of water from Funka Bay, Hokkaido, during early spring, *J. Oceanogr. Soc. Jpn*., *44*, 163–170, 1988.

Molcard, R., Preliminary results of current measurements in the Strait of Sicily in May 1970, *Proc. SACLANT Conf*., 7th, 82–95, 1972.

Morel, A., Caractères hydrologiques des eaux échangés entre le bassin oriental et le bassin occidental de la Méditerranée, *Cah. Oceanogr*., *22*(3), 329–342, 1971.

Nof, D., Choked flows from the Pacific to the Indian Ocean, *J. Phys. Oceanogr*., *25*, 1369–1383, 1995a.

Nof, D., Choked flows and wind-driven interbasin exchange, *J. Mar. Res*., *53*, 23–48, 1995b.

Nof, D., and D. Olson, On the flow through broad gaps with application to the Windward Passage, *J. Phys. Oceanogr*., *13*, 1940–1956, 1983.

Pedlosky, J., *Geophysical Fluid Dynamics*, 624 pp., Springer-Verlag, New York, 1979.

Petren, O., and G. Walin, Some observations of the deep flow in the Bornholm Strait during the period June 73–December 74, *Tellus*, *28*(1), 74–87, 1976.

Polzin, K. L., K. G. Speer, J. M. Toole, and R. W. Schmitt, Intense mixing of Antarctic Bottom Water in the equatorial Atlantic Ocean, *Nature*, *380*, 54–57, 1996.

Pratt, L. J., On inertial flow over topography, 1, Semigeostrophic adjustment to an obstacle, *J. Fluid Mech*., *131*, 195–218, 1983.

Pratt, L. J., On inertial flow with multiple observations, *J. Atmos. Sci*., *41*, 1214–1224, 1984a.

Pratt, L. J., On inertial flow over topography, 2, Rotating channel flow near the critical speed, *J. Fluid Mech*., *145*, 95–110, 1984b.

Pratt, L. J., Hydraulic control of sill flow with bottom friction, *J. Phys. Oceanogr*., *16*, 1970–1980, 1986.

Pratt, L. J., and L. Armi, Hydraulic control of flows with nonuniform potential vorticity, *J. Phys. Oceanogr*., *17*, 2016–2029, 1987.

Pratt, L. J., and P. A. Lundberg, Hydraulics of rotating strait and sill flow, *Annu. Rev. Fluid Mech*., *23*, 81–106, 1991.

Reid, J. L., and P. F. Lonsdale, On the flow of water through the Samoan Passage, *J. Phys. Oceanogr*., *4*, 58–73, 1974.

Rudnick, D., Direct velocity measurements in the Samoan Passage, *J. Geophys. Res*., *102*, 3293–3302, 1997.

Rydberg, L., Rotating hydraulics on deep-water channel flow, *Tellus*, *32*, 77–89, 1980.

Sambuco, E., and J. A. Whitehead Jr., Hydraulic control by a wide weir in a rotating fluid, *J. Fluid Mech*., *73*, 521–528, 1976.

Saunders, P. M., Flow through Discovery Gap, *J. Phys. Oceanogr*., *17*, 631–643, 1987.

Saunders, P. M., Cold outflow from the Faeroe Bank Channel, *J. Phys. Oceanogr*., *20*, 29–43, 1990.

Saunders, P. M., The flux of overflow water through the Charlie-Gibbs Fracture Zone, *J. Geophys. Res*., *99*, 12,343–12,355, 1994.

Shen, C. Y., The rotating hydraulics of open-channel flow between two basins, *J. Fluid Mech*., *112*, 161–188, 1981.

Speer, K. G., and W. Zenk, The flow of Antarctic Bottom Water into the Brazil Basin, *J. Phys. Oceanogr*., *23*, 2667–2682, 1993.

Stalcup, M. C., W. G. Metcalf, and R. G. Johnson, Deep Caribbean inflow through the Anegada-Jungfern Passage, *J. Mar. Res*., *33*, suppl., 15–35, 1975.

Stern, M. E., Hydraulically critical rotating flow, *Phys. Fluids*, *15*, 2062–2065, 1972.

Stern, M. E., Geostrophic fronts, bores, breaking and blocking waves, *J. Fluid Mech*., *99*, 687–704, 1980.

Stern, M. E., J. A. Whitehead, and B. L. Hua, The intrusion of a density current along a coast of a rotating fluid, *J. Fluid Mech*., *123*, 237–265, 1982.

Toulany, B., and C. Garrett, Geostrophic control of fluctuating barotropic flow through straits, *J. Phys. Oceanogr*., *14*, 649–655, 1984.

Vangriesheim, A., Antarctic bottom water flow through the Vema Fracture Zone, *Oceanol. Acta*, *3*, 199–207, 1980.

Whitehead, J. A., Flow of a homogeneous rotating fluid through straits, *Geophys. Astrophys. Fluid Dyn*., *36*, 187–205, 1986.

Whitehead, J. A., Internal hydraulic control in rotating fluids—Applications to oceans, *Geophys. Astrophys. Fluid Dyn*., *48*, 169–192, 1989.

Whitehead, J. A., and R. Kimura, Rotating hydraulic models of fronts at the continental shelf break and in circular eddies, *Geophys. Astrophys. Fluid Dyn*., *76*, 1–27, 1994.

Whitehead, J. A., and D. L. Porter, Axisymmetric critical withdrawal of a rotating fluid, *Dyn. Atmos. Oceans*, *2*, 1–18, 1977.

Whitehead, J. A., Jr., and L. V. Worthington, The flux and mixing rates of Antarctic Bottom Water within the North Atlantic, *J. Geophys. Res*., *87*, 7903–7924, 1982.

Whitehead, J. A., A. Leetmaa, and R. A. Knox, Rotating hydraulics of strait and sill flows, *Geophys. Fluid Dyn*., *6*, 101–125, 1974.

Yih, C. S., *Stratified Flows*, 418 pp., Academic, San Diego, Calif., 1980.

J. A. Whitehead, Department of Physical Oceanography, Mail Stop 21, Woods Hole Oceanographic Institution, Woods Hole, MA 02543-1541. (e-mail: jwhitehead@whoi.edu)